Calculating Phase Diagrams of Polymer−Platelet Mixtures Using Density Functional Theory: Implications for Polymer/Clay Composites

Valeriy V. Ginzburg and Anna C. Balazs*

Department of Chemical and Petroleum Engineering, University of Pittsburgh, Pittsburgh, Pennsylvania 15261

Received January 29, 1999; Revised Manuscript Received June 10, 1999

ABSTRACT: We analyze the thermodynamics of disklike particles dispersed in a polymer matrix. Using the Somoza−Tarazona free energy functional for thin oblate ellipsoids of revolution in combination with the Flory−Huggins mixing free energy, we obtain a new expression that allows us to describe the complete (liquid, crystalline, and liquid crystalline) phase diagram for the mixture as a function of shape anisotropy κ, polymer chain length N, and the disk−disk interaction parameter, q. It is shown that at large q and/or N positional ordering plays an important role in determining the stability and morphology of such mixtures.

Introduction

In recent years, polymer−clay nanocomposites have generated significant interest due to their remarkable mechanical, thermal, and barrier properties.[1−12] Such materials typically consist of nanoscale clay particles dispersed in a polymer matrix. The typical weight fractions of clay are less than 10%, which make the materials lighter than most conventional composites. While there has been significant progress in fabricating thermodynamically stable polymer−clay mixtures, there has been less progress in isolating the factors that govern the kinetic[7] and thermodynamic[12] behavior of these mixtures.

Establishing a thermodynamic description of polymer−clay mixtures is related to the more general problem of determining the phase behavior of polymer−colloid mixtures. The thermodynamics of polymer−colloid mixtures has been the subject of numerous theoretical, computational, and experimental studies.[13−18] In most of the theoretical and computational investigations, the colloidal particles were assumed to be spherical in shape, and the Asakura−Oosawa[13] model was adopted to describe the polymer−colloid mixture. In the latter model, the polymers are represented by small spheres, and the only interaction is due to excluded-volume effects. Thus, the problem of characterizing the complex blend was reduced to describing the properties of a binary hard-sphere mixture. The phase diagram of binary hard-sphere mixtures can be calculated to obtain liquid and solid (colloidal crystal) phases. Calculated phase diagrams can be then tested against experimental data, and good qualitative agreement is generally found between theory and experiment for mixtures of spherical colloids and polymers.[19,20]

In the case of polymer−clay mixtures, however, a complicating factor is introduced by the strong anisotropy in the shape of the clay particles. A typical clay "sheet" is approximately 100−200 nm in diameter and approximately 1 nm in thickness. Because of this high degree of anisotropy, clay particles experience orientational ordering at low volume fractions and can form liquid crystalline phases (nematic, smectic, or columnar), in addition to traditional liquid and solid phases (see Figure 1). Although there have been a few numerical and experimental studies of the thermodynamics of mixtures containing anisotropic colloidal particles,[21−23] most of these investigations were focused on rodlike colloids, rather than diskotic particles. Monte Carlo simulations performed by Dijkstra et al.[24] did specifically analyze the phase behavior of clay particles (modeled as infinitely thin disks with quadrupolar potentials), but these studies were in the absence of solvent or polymer. The major challenge in developing models for the phase behavior of polymer−clay mixtures is correctly treating the strong structural anisotropy of the sheets and properly characterizing all possible mesophases of the mixture.

Recently, Lyatskaya and Balazs[25] proposed a simple model that describes the nematic ordering in the polymer−clay systems. Starting from the Onsager[26] free energy functional for the nematic ordering of rigid rods, they developed a modified expression to combine the disk orientational and positional entropy, steric excluded-volume effects, translational entropy of the polymer, and the Flory−Huggins enthalpic interaction. The resulting isotropic−nematic phase diagram correctly represents many important features, such as the role of shape anisotropy in depressing the ordering transition and the increase in the size of the immiscibility region with increases in the polymer chain length. Unlike most of the phenomenological theories of polymer−liquid crystal systems,[27−29] in the Onsager-type model the features of the phase diagram are directly derived from the geometric characteristics of the anisotropic component.

In this paper, we modify and expand the above theory[25] to include smectic, columnar, and crystalline phases. In carrying out these calculations, we adopt the Somoza−Tarazona[30,31] formalism of the density functional theory (DFT) and incorporate expressions that describe the entropy of mixing between the different components and the enthalpic interactions between the disks. The resulting free energy functional can be minimized with respect to both the orientational and positional single-particle distribution function of the disks, and thus, potentially, all phases and coexistence regions can be determined. We obtain, for the first time, the isotropic−nematic−crystal phase diagram for oblate hard ellipsoids in a broad range of shape anisotropies and study the role played by the polymer chain length

10.1021/ma990135t CCC: $18.00 © 1999 American Chemical Society
Published on Web 08/05/1999

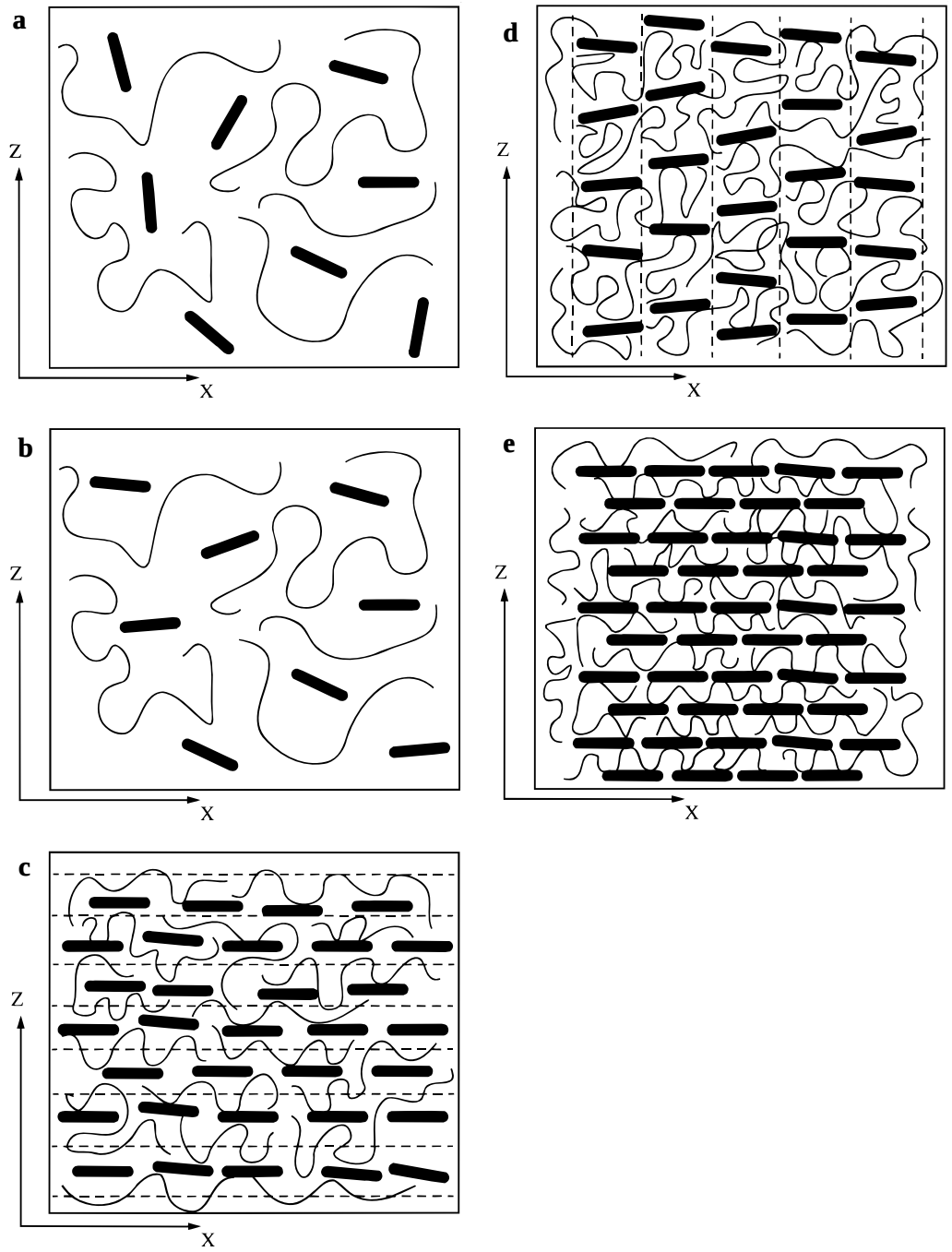

Figure 1. Possible mesophases of oblate uniaxial particles dispersed in a polymer: (a) isotropic, (b) nematic, (c) smectic A, (d) columnar, and (e) crystal. The nematic director **n** in ordered phases is aligned along *Z* axis; the disks lie in the *XY* plane. Dashed lines show smectic layers (c) and columns (d).

and the interparticle interactions in modifying this phase behavior. While in the above discussion we mostly concentrated on polymer−clay composites, the theory described below is applicable to other polymer−colloid mixtures. In particular, this model is especially useful for composites that contain high aspect ratio fillers, such as fibers or mica sheets.

Free Energy Density Functional

The density functional approach, first formulated by Ramakrishnan and Yussouf,[32] is based on the theorem that the free energy of a system can be written as a functional of the single-particle distribution function (SDF). For spherical particles, the SDF is a function only of the coordinate **r**; for rigid anisotropic objects, the SDF is a function of both **r** and the nematic director **n**. The free energy is typically written in the form

$$\beta F = \beta F_{\mathrm{id}} + \beta F_{\mathrm{ster}} + \beta F_{\mathrm{int}} \qquad (1)$$

where F_{id} is the free energy of an "ideal gas" of colloidal particles and polymers, F_{ster} is the contribution due to the excluded-volume effects for the colloidal (clay) particles, F_{int} represents the enthalpic (attractive or repulsive) interactions between clay particles, and $\beta = 1/kT$.

We assume, as in ref 25, that the fluid is incompressible; i.e., the sum of volume fractions of polymer, ϕ_{p}, and clay, ϕ_{c}, equals 1, thus $\phi_{\mathrm{p}} = 1 - \phi_{\mathrm{c}}$. This condition allows

us to express all properties in terms of the particle SDF $\gamma(\mathbf{r},\mathbf{n})$. To simplify calculations, we decouple orientational and translational degrees of freedom in the SDF:

$$\gamma(\mathbf{r},\mathbf{n}) = \rho(\mathbf{r})\, f(\mathbf{n}) \tag{2}$$

where $\rho(\mathbf{r})$ is a number density of the disks, and $f(\mathbf{n})$ is the Onsager orientational distribution function. This decoupling approximation was first suggested by Kventsel et al.[33] to describe the isotropic−nematic−smectic A phase diagram for thermotropic liquid crystals. For the spatially uniform isotropic and nematic phases, $\rho(\mathbf{r}) = \rho =$ constant, and the density functional model reduces to the familiar Onsager theory of the nematic−isotropic transition.

Assuming that the orientational ordering of the disks does not influence the "ideal" (Flory−Huggins) entropy of mixing, we can write the first term of eq 1 as

$$\beta F_{\mathrm{id}} = \int \mathrm{d}\mathbf{r} \left[\rho(\mathbf{r}) \ln(v_{\mathrm{c}}\rho(\mathbf{r})) + \rho(\mathbf{r}) \int \mathrm{d}\mathbf{n}\, f(\mathbf{n}) \times \ln(4\pi f(\mathbf{n})) + \frac{1}{N v_{\mathrm{m}}}(1 - \rho(\mathbf{r})v_{\mathrm{c}}) \ln(1 - \rho(\mathbf{r})v_{\mathrm{c}}) \right] \tag{3}$$

where N is the chain length of the polymer, and v_{m} and v_{c} are the volumes of a monomer and clay particle, respectively. Here, the first and third terms describe the translational entropy of the disks and polymers, respectively. The second term describes the orientational entropy of the disks.

In writing the ideal mixing (Flory−Huggins) free energy contribution for the polymer, we assumed that the chains are flexible and that the monomer units are spherical in shape. In this case, chains have no orientational free energy contribution. The configurational free energy of the polymer is not coupled to the orientational ordering of the disks; it must, however, be strongly coupled to the positional ordering of the disks, since the formation of layers strongly reduces the number of possible configurations for polymer chains. For relatively low volume fractions of disks, most polymer chains interact with no more than two clay particles. Thus, the configurational free energy of the polymer can be thought of as part of the effective disk−disk pair potential. A calculation of this polymeric contribution can be done, for example, using the self-consistent field (SCF) method of Scheutjens and Fleer[34−36] and will be the subject of future work.[37] In this paper, we simply postulate a functional form for the total disk−disk interaction potential, assuming that it incorporates both the long-range interaction between bare disks and the configurational free energy of polymer chains confined between these disks.

Up to this point, we have not specified the shape of the particles under consideration, assuming only that they are uniaxial (i.e., possess at least cylindrical symmetry). We now assume that each particle is an oblate ellipsoid of revolution, characterized by its diameter σ_0 and thickness σ_z. (Although cut spheres or cylinders would be a more natural choice to describe the clay particles, the DFT equation of state is quasi-exact for ellipsoids.[30] To apply this formalism to cylinders or cut spheres, it is necessary to modify the nonideal steric term βF_{ster}, which will be the subject of future studies.) The shape anisotropy parameter is $\kappa = \sigma_z/\sigma_0 \leq 1$. For such a system, a semiempirical steric interaction free energy can be written as[30,31,38,39]

$$\beta F_{\mathrm{ster}} = \int \mathrm{d}\mathbf{r}\, \rho(\mathbf{r})\, \Psi_{\mathrm{hs}}(\bar{\phi}_{\mathrm{c}}(\mathbf{r})) \frac{V_{\mathrm{excl}}[f]}{V_{\mathrm{phe}}} \tag{4}$$

where $\Psi_{\mathrm{hs}}(x)$ is the semiempirical Carnahan−Starling[40] function, which describes the excess (nonideal) free energy density for hard spheres as a function of their packing fraction. The parameter $V_{\mathrm{excl}}[f]$ is the average excluded volume per particle for a given orientational distribution, and V_{phe} is the excluded volume per particle for perfectly aligned ellipsoids. If we consider only spatially uniform phases (e.g., isotropic and nematic phases), eq 4 would reduce to the Onsager-type expression with the correct second virial coefficient. For nonuniform phases, it is a complicated functional of the density, because the function $\bar{\phi}_{\mathrm{c}}(\mathbf{r})$ depends on $\rho(\mathbf{r})$ in a nontrivial manner. (For more details see Appendix A and refs 30 and 31.) The role of this functional is to properly describe the short-range correlations due to the excluded-volume interactions.

The sum of the free energy terms in eqs 3 and 4 describes an athermal dispersion of hard ellipsoids in a polymer matrix. It is known that such a system is capable of forming liquid crystalline (nematic) and crystalline phases.[22,42] To obtain additional liquid crystalline phases (smectic or columnar), strongly anisotropic long-range interactions are required.[41]

We suppose that the interaction free energy, βF_{int}, is "small" compared to the ideal and steric free energy terms, i.e., $|\beta F_{\mathrm{int}}| < |\beta F_{\mathrm{id}} + \beta F_{\mathrm{ster}}|$.[43] In this case, one can assume that the pair correlation function for the particles, $g(1,2)$, is mostly determined by the excluded-volume effects (not long-range interactions) and calculate the interaction free energy βF_{int} as

$$\beta F_{\mathrm{int}} = {}^1/_2 \int \mathrm{d}\boldsymbol{r}_1\, \mathrm{d}\boldsymbol{r}_2\, \mathrm{d}\mathbf{n}_1\, \mathrm{d}\mathbf{n}_2\, \rho(\boldsymbol{r}_1)\, \rho(\boldsymbol{r}_2)\, f(\mathbf{n}_1)\, f(\mathbf{n}_2) \times \delta(1 - \mathbf{n}_1 \cdot \mathbf{n}_2)\, g(1,2)\, V(\boldsymbol{r}_1 - \boldsymbol{r}_2) \tag{5}$$

where the mean-field pair correlation function $g(1,2) = 0$, if particles overlap, and is equal to 1, if they do not overlap. This form is similar to the traditional way of representing enthalpic interactions between anisotropic particles (see, e.g., eq 3 in ref 39). The δ-function in the rhs of eq 5 allows only those configurations in which interacting disks are parallel. Such an approximation is reasonable for very anisotropic particles where side-by-side configurations have significantly larger "contact" area than either side-to-edge or edge-to-edge configurations. In addition, since this potential is highly anisotropic, it is likely to promote the formation of smectic and columnar phases.

We take the potential function $V(\boldsymbol{r}_1 - \boldsymbol{r}_2)$ to be of the form

$$V(\mathbf{r}) = -A\, q \left(1 - \left(\frac{r_\perp}{\sigma_0}\right)^2\right) \sin((\pi/D)((z/\sigma_z) - 1)), \quad \text{if } 0 < r_\perp < \sigma_0 \text{ and } \sigma_z < |z| < \sigma_z(1 + D)$$

$$= 0, \text{ otherwise}$$

where A is the disk surface area and q is the interaction energy density parameter. This form is selected because it conveniently parametrizes a single attractive well or a single repulsive barrier between the two disks and allows for a simple analytical Fourier transformation,

which significantly speeds up the calculation. The dimensionless parameter D describes the relative width of an attractive well (if $q > 0$) or a repulsive barrier (if $q < 0$) compared to the disk thickness σ_z. We set $D = \sigma_z$ for all our calculations.

As discussed above, the potential $V(\mathbf{r})$ implicitly models the effect of the following two contributions: (i) the attraction or repulsion between bare clay sheets and (ii) the attraction or repulsion due to the change in the configurational free energy of the polymer chains between the sheets. The interaction parameter q describes the combined effect of both contributions. If $q > 0$, clay particles attract each other and repel the polymer (corresponding to a positive Flory−Huggins parameter χ between the polymer and the clay); if $q < 0$, clay particles repel each other (negative χ between the polymer and the clay). The case of $q = 0$ describes the situation where the only interaction between the clay particles is due to the excluded-volume effects.

To describe the thermodynamic behavior of the system, it is necessary to minimize the free energy for all possible phases (isotropic, nematic, smectic, columnar, and crystal) for each value of ϕ_c and find the lowest energy state. After that, coexistence regions can be found by means of applying the Maxwell rule or, equivalently, by equating the chemical potentials of the particles and the polymer for the different phases. The minimization is done using a variational approach in which the SDF is parametrized by specific functions that reflect the symmetry of a given phase. We use the following parametrization.

For orientational SDF:

$$f(\mathbf{n}) = \frac{\alpha}{4\pi \sinh \alpha} \cosh(\alpha \cos(\mathbf{n},\mathbf{z})) \tag{6}$$

For positional SDF:

$$\rho(\mathbf{r}) = \rho A \exp(L \cos(Q_z z)), \quad \text{for the smectic A phase} \tag{7}$$

$$\rho(\mathbf{r}) = \rho A \exp(L \cos(Q_x x) \cos(Q_y y)), \quad \text{for the columnar phase} \tag{8}$$

$$\rho(\mathbf{r}) = \rho A \exp(L \cos(Q_x x) \cos(Q_y y) \cos(Q_z z)), \quad \text{for the crystal phase} \tag{9}$$

In each case, A is a normalization constant, while L describes the strength of the positional ordering. To minimize the number of free parameters, we assume that the columnar structure is hexagonal ($Q_x = \sqrt{3}Q_y$), and the crystal structure is "stretched" hexagonal close packed ($Q_x = \sqrt{3}Q_y = \kappa\sqrt{3}Q_z$).

The set of equations determining equilibrium phases, phase boundaries, and coexistence regions is solved numerically for each specific set of parameters. Below, we present resulting phase diagrams for various values of the shape anisotropy κ, the polymer chain length N, and the interaction parameter q.

Results

Hard-Core Interactions ($q = 0$). It is well established[42,44] that in the absence of attractive forces ellipsoidal particles do not form smectic or columnar phases, only isotropic, nematic, and crystal ones. The introduction of polymer or a variation in the shape anisotropy parameter is not expected to change the structure of a phase diagram; however, it may significantly alter the actual values of the phase coexistence boundaries. Indeed, the volume fraction at which the nematic−isotropic transition occurs is proportional to the shape anisotropy κ, at least in the limit $\kappa \to 0$.[26]

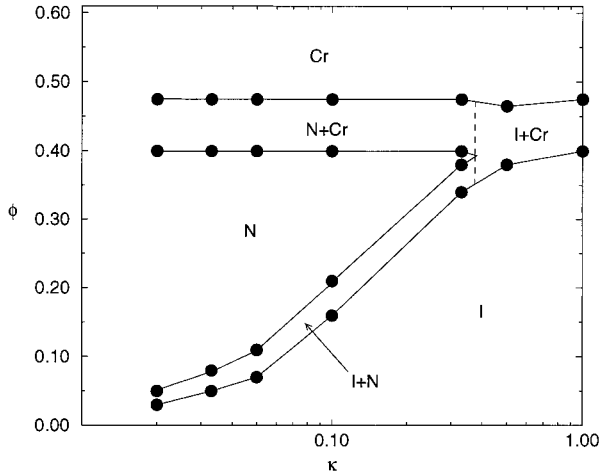

Figure 2. Phase diagram of hard oblate ellipsoids dispersed in a polymer with the chain length $N = 1000$ and the monomer volume $v_m = 0.005v_c$ as a function of the shape anisotropy κ. Calculations are done for $\kappa = 1$, 0.5, 0.33, 0.1, 0.05, 0.033, and 0.02; lines between these points are drawn as guide for the eye. Dashed line represents the three-phase coexistence. Phases: I, isotropic; N, nematic; Cr, crystal.

We calculate the phase diagram for a broad set of shape anisotropies $\kappa = 1$, 0.5, 0.33, 0.1, 0.05, 0.033, and 0.02. Note that as κ is decreased, the anisotropy increases. For each value of κ, the volume fraction ϕ_c is varied between 0.01 and 0.60 with increments of 0.01. To evaluate the free energy for the crystal phase, we used a spatial lattice that has 16 sites per crystal period.[46]

In Figure 2, the ϕ_c versus κ phase diagram is plotted for the case $N = 1000$. The volume of a monomer v_m is taken to be $0.005v_c$, where v_c is the volume of a clay particle. (Such a ratio is typical for polymer−clay mixtures, where the characteristic monomer volume is on the order of 1 nm^3 or less, while a clay particle has a volume of hundreds of cubic nanometers.) In the limit of high chain length, polymer entropy becomes negligible, and the phase diagram is very similar to that of hard ellipsoids in a vacuum.[42,44] For strongly anisotropic systems ($\kappa \ll 1$), the two transitions (isotropic−nematic and nematic−crystal) become well-separated and distinct. The nematic−isotropic transition is well described by the Onsager approximation, while the nematic−crystal transition is well described by the model of "perfectly aligned ellipsoids", since the nematic order parameter is close to 1 near crystallization densities. According to Frenkel,[44] the nematic−crystal transition is similar to the hard-sphere crystallization, and indeed, we observe that the transition densities are the same for $\kappa = 1$, the case of hard spheres, and for all $\kappa < 0.1$. The actual value of the transition densities ($\phi_i = 0.41$, $\phi_c = 0.48$) are slightly lower than the known data for the hard-sphere fluid ($\phi_i = 0.49$, $\phi_c = 0.55$; see, e.g., ref 19). (Here, subscripts refer to the type of phase: i = isotropic, c = crystal). This discrepancy arises from numerical errors in the calculation of the crystal free energy and can be reduced by increasing the number of grid points per unit cell.

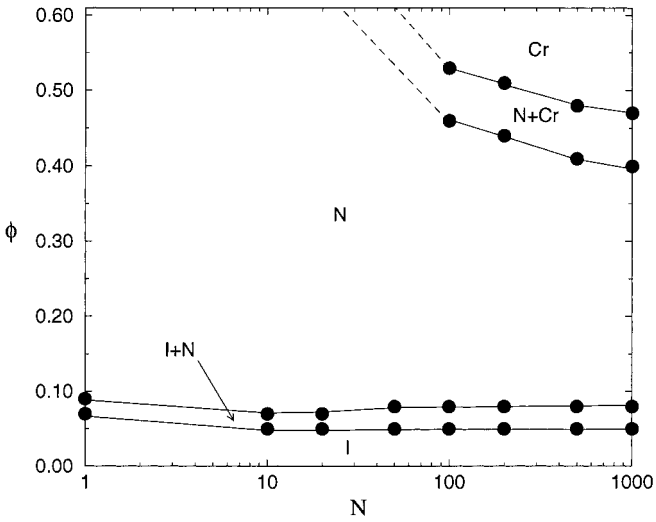

Figure 3. Phase diagram of hard oblate ellipsoids with shape anisotropy $\kappa = 0.033$ as a function of the polymer chain length N. Calculations are done for $N = 1$, 10, 20, 50, 100, and 1000; lines between these points are drawn as guide for the eye. Dotted lines are extrapolation to the region where DFT breaks down. Phases: as in Figure 1.

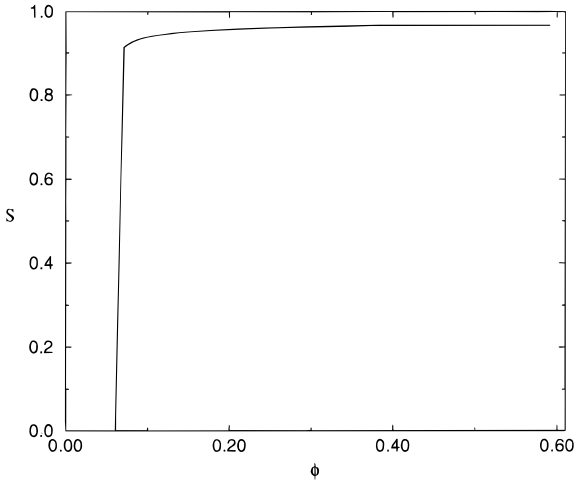

Figure 4. Nematic order parameter as a function of volume fraction for disks with $\kappa = 0.033$ in a monomeric solvent ($N = 1$).

To study the dependence of the phase behavior on the polymer chain length, we calculate the phase diagram as a function of N for the selected value of $\kappa = 0.033$. Results are presented in Figure 3. It can be seen that an increase in chain length reduces the density of the nematic−crystal transition, while leaving the nematic−isotropic transition unchanged. For short chains, we do not observe the nematic−crystal transition at all. This effect can be easily understood: in a small-molecule solvent, steric and energetic gains from the positional ordering of the disks are smaller than the loss of translational entropy for solvent molecules.

To show that the disks have a strong orientational ordering in the nematic phase, in Figure 4 we plot the nematic order parameter $S = 0.5\langle 3\cos^2(\mathbf{n},\mathbf{z}) - 1\rangle$ as a function of the particle volume fraction for the particle dispersion in a monomeric solvent ($\kappa = 0.033$, $N = 1$). It can be seen that the change in the value of S at the nematic−isotropic transition is very large (≈0.90). This jump in S is close to the Onsager result ($S = 0.84$) for infinitely long rods. In real systems, observed values of the nematic order parameter are usually lower; it is known that mean-field theories overestimate nematic ordering but predict the location of the nematic−isotropic transition rather accurately.[45]

It is important to note that the phase diagrams depend on the selected particle shape. Since in our calculation the colloidal particles are assumed to be ellipsoids, no smectic or columnar phases are observed. For cylindrical particles, it is expected that smectic or columnar phase may preempt the crystal phase in some narrow range of densities. These partially ordered phases have indeed been observed in many colloidal systems,[22] including polymer−clay mixtures.[8] Also, shape fluctuations due to bend or splay deformations may lead to the appearance of liquid crystalline mesophases instead of a crystalline phase. Finally, some of these mesophases may be induced by enthalpic interactions, as we discuss below.

Enthalpic Interactions. To determine how the strength of the disk−disk potential affects the phase behavior, we calculated phase diagrams for several systems with different interaction strengths and polymer chain lengths. The aspect ratio of the disks is fixed at $\kappa = 0.033$, while the interaction strength q is varied between −0.02 and +0.02 (in units of kT per one monomer lattice site). The interaction free energy is of the form given in eq 5. When evaluating the integral over positions and orientations of particles, the orientational lattice approximation (see, e.g., ref 47) is used, in which particle orientations are restricted to being along the x, y, or z directions only. This approximation is necessary to reduce the number of degrees of freedom and thus make it possible to analyze the whole phase diagram within a reasonable time frame. (The errors introduced by using the orientational lattice cannot significantly alter the phase diagram since they contribute only to βF_{int} and not to the dominant term βF_{ster}; however, it is possible that the use of the orientational lattice approximation slightly affects the equilibrium value of the nematic order parameter in the ordered phase.) We vary the polymer chain length $N = 10$, 20, 50, 100, and 1000 monomer units. Calculated phase diagrams are depicted in Figure 5a−e.

It can be seen that the topology of the phase diagram (phases and their boundaries) is significantly affected by both the chain length and the strength of the potential. For a very short chain ($N = 10$, Figure 5a), within the examined interaction range, no positional ordering is observed. The only phase transition that occurs is the isotropic−nematic transition with a relatively narrow biphasic region. This indicates, as expected, that for short organic solvents positional ordering does not occur. (This type of ordering would entail significant entropic losses for the solvent molecules.) Thus, such colloidal solutions are almost always uniform.

As the chain length is increased ($N = 20$, Figure 5b), we observe the onset of positional ordering for large positive and negative values of q. For the case of strong attraction between disks, the crystalline structure begins to form at high volume fractions ($\phi = 0.53$). For the case of strong repulsion, the ordering starts at $\phi = 0.35$, but the ordered phase is not crystalline, but columnar. Ordering disappears for small values of q, so at $q = 0$, only isotropic and nematic phases are seen. When the polymer chain length is increased even further ($N = 50$, Figure 5c), we can also see the appearance of a smectic A (lamellar) phase in a narrow

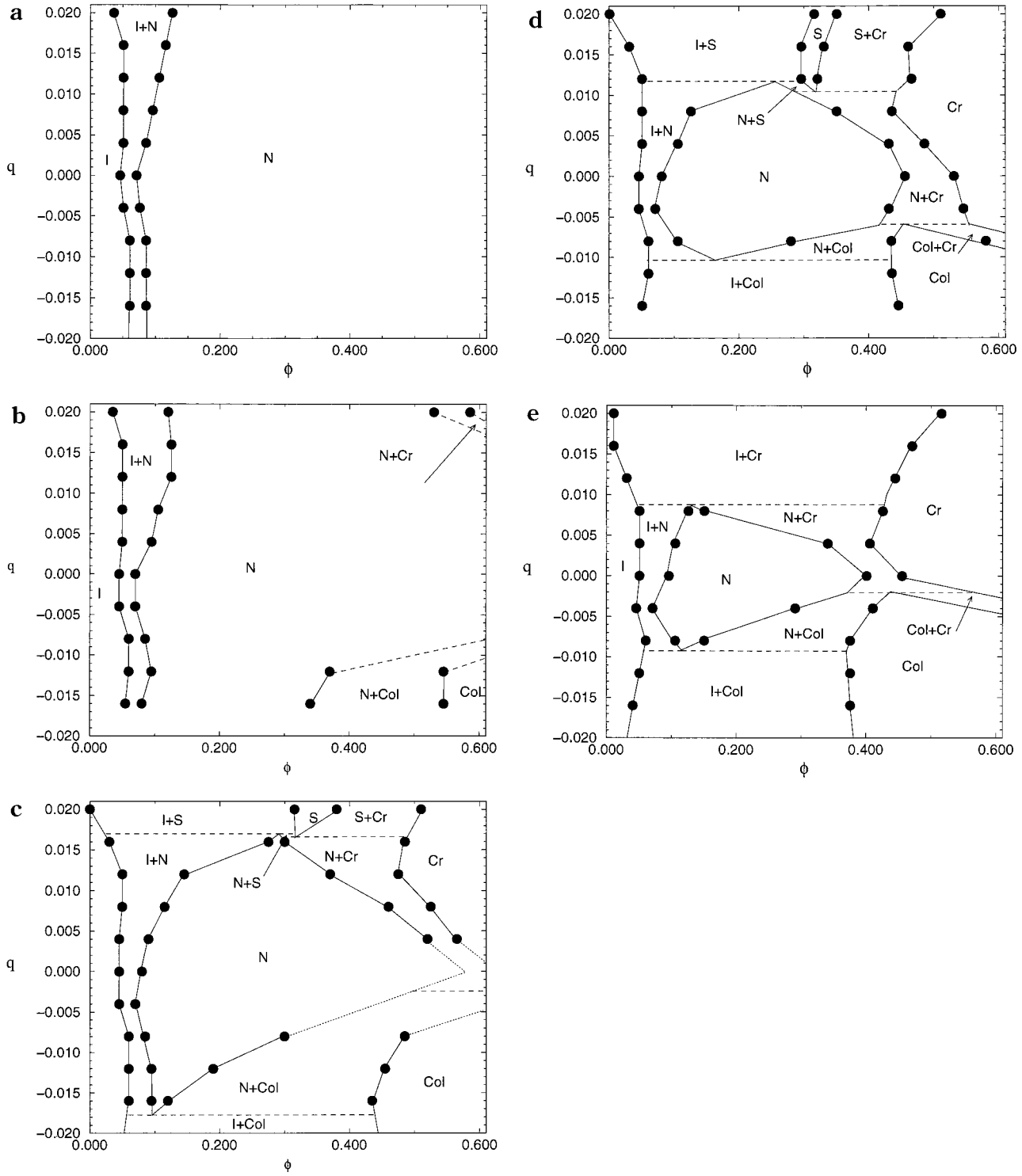

Figure 5. Phase diagram of the mixture of ellipsoidal particles with an ideal polymer. Particle shape anisotropy $\kappa = 0.033$. Interparticle free energy is given by eq 5. Phases: I, isotropic; N, nematic; S, smectic A (lamellar); Col, columnar; Cr, crystal. Chain length $N = 10$ (a), 20 (b), 50 (c), 100 (d), and 1000 (e). Lines serve as guide to the eye; dotted lines are extrapolations, and dashed lines indicate three-phase coexistence.

region ($0.017 \leq q \leq 0.020$, $0.30 \leq \phi \leq 0.35$). The layer spacing in this smectic phase equals $1.45\sigma_z$, very close to the minimum of the pair potential ($1.5\sigma_z$). In addition, one can also observe the isotropic−nematic−smectic triple point for the attractive potential and the isotropic−nematic−columnar triple point for the repulsive potential. In both cases, as the strength of the potential is increased, the coexistence between the isotropic phase and the positionally ordered (smectic or columnar) phase becomes broader.

For high chain lengths ($N = 100$, Figure 5d, and $N = 1000$, Figure 5e), the nematic region becomes even more narrow, while the isotropic−nematic−smectic (isotropic−nematic−crystal for the case $N = 1000$) and isotropic−nematic−columnar triple points move toward the line $q = 0$. This indicates that even for a small attraction or repulsion between the disks, spatially uniform phases would become unstable, moving toward the formation of lamellae-like structures (if there is an attraction) or toward columnar-type ordering (if there is a repulsion).

Interestingly, the smectic phase seems to disappear for the $N = 1000$ case, suggesting that for this system the crystalline ordering is favored even at relatively small volume fractions of disks.

One should note the formation of the positionally ordered (columnar) phase in the limit of strong repulsion. This effect is somewhat similar to the formation of charge-stabilized colloidal crystals.[48] The repulsive interactions effectively increase the excluded volume and thus make the positional ordering occur at lower volume fractions. In the case of a highly anisotropic repulsive potential this apparently leads to the formation of the columnar phase, where the disks become close-packed in the XY plane but well-separated along Z direction.

It is important to mention that the topology of the phase diagram is sensitive to the exact form of the interaction potential. It was shown by de Miguel et al.[49,50] that, for prolate particles interacting via the Gay−Berne potential,[51] changing the energy anisotropy of the potential leads to the appearance or disappearance of the smectic A phase. Although no such systematic studies were performed for oblate particles (the simulations of Gay−Berne disks, performed by Bates and Luckhurst,[52] do not address the role of the energy anisotropy), similar effects clearly should be seen for the disks as well.

The calculated phase diagrams clearly show that an increase in the polymer chain length leads to a decrease in miscibility between the disks and the polymer and to the segregation and the formation of ordered phases (smectic, columnar, or crystal). Although the model does not treat the configurational entropy of the polymer chains explicitly, including the proper description of these contributions would only reinforce our conclusions. (In particular, the losses in the configurational entropy for long chains would promote phase separation between the polymer and clay.) The positional ordering can also be produced by a strong interaction between filler particles (no matter whether this interaction is caused by electrostatics, depletion, or van der Waals forces). Furthermore, no matter whether the potential between particles is attractive or repulsive, the nematic phase eventually becomes unstable toward some positional ordering as the chain length is increased. Thus, to achieve a locally uniform structure (isotropic or nematic phase), it is important to make the effective long-range interaction between the clay particles as neutral as possible. In practical terms, such structures could be observed only if the effective polymer−clay Flory−Huggins parameter χ (which is directly proportional to the interaction strength q) is close to zero, and the polymer chain length N is not extremely high. For high values of N and/or χ, one would always observe some degree of ordering on a nanoscale level, either due to the two-phase coexistence or because of the formation of ordered (smectic or crystalline) phases.

Conclusions

We develop a model based on perturbation-type density functional theory to describe the complete (liquid, crystal, and liquid crystal) phase diagram of an incompressible polymer−disk mixture. The phase diagram is shown to exhibit a strong dependence on the shape anisotropy of the filler particles, the polymer chain length, and the strength of the interparticle interaction. In particular, an increase in the shape anisotropy for oblate ellipsoidal filler particles leads to the broadening of the nematic phase at the expense of the isotropic region. The increase in the polymer chain length leads to the formation of the crystalline and/or liquid crystalline mesophases and promotes segregation between polymer-rich regions and filler particles. Finally, an increase in the strength of the interparticle potential leads to the complete elimination of the nematic phase and to the direct coexistence between isotropic and crystal or columnar phases. Even though our results are semiqualitative in the limit of intermediate and high volume fractions of colloidal particles, they capture the topology of the phase diagram and the nature of the ordered phases. This knowledge can be used in the design and development of new polymer composites.

The proposed model also allows us to use molecular theories to directly relate phase diagrams to specific characteristics of the polymers and clays. For clay particles dispersed in a polymer melt, the effective interparticle potentials can be calculated using the self-consistent-field (SCF) model of Fleer and Scheutjens.[34−36] Thus, it is possible to establish a correlation between the phase diagram and the architecture of grafted or adsorbed chains. This correlation would be important in determining morphology and predicting physical properties of polymer−clay composites. Such calculations are currently underway.[37]

Acknowledgment. We thank Drs. Chandralekha Singh and Yulia Lyatskaya for fruitful discussions. A.C.B. gratefully acknowledges the financial support of the Army Office of Research, the DOE through Grant DE-FG02-90ER45438, and The Dow Chemical Company. We also thank anonymous referees for helpful suggestions.

Appendix. Smoothed Density Approximation

The smoothed density functional $\bar{\phi}(\mathbf{r})$ is given by

$$\bar{\phi}(\mathbf{r}) = v_c\bar{\rho}(\mathbf{r}) = v_c\int d\mathbf{R}\ \rho(\mathbf{r})\ w(|\mathbf{r} - \mathbf{R}|, \bar{\rho}) \quad \text{(A1)}$$

where the normalized weight function $w(|\mathbf{r} - \mathbf{R}|, \bar{\rho})$ is used to smooth (coarse-grain) density variations. For ellipsoids, it is given by

$$w(|\mathbf{r}|, \bar{\rho}) = w_0(|\mathbf{s}|) + \bar{\rho}w_1(|\mathbf{s}|) + \bar{\rho}^2w_2(|\mathbf{s}|) \quad \text{(A2)}$$

where $\mathbf{s}$ is the normalized distance defined by $\mathbf{r} = \mathbf{\Sigma s}$ ($\mathbf{\Sigma}$ is diagonal matrix whose elements are three lengths of the ellipsoid σ_x, σ_y, σ_z). Functions $w_0(s)$, $w_1(s)$, and $w_2(s)$ are derived in ref 31. Equations A1 and A2 are nonlinear and must be solved numerically to determine the smoothed profile $\bar{\rho}(\mathbf{r})$ for any given single-particle density $\rho(\mathbf{r})$.

References and Notes

(1) Giannelis, E. P.; Krishamoorti, R.; Manias, E. *Adv. Polym. Sci.* **1999**, *138*, 107 and references therein.
(2) Hacket, E.; Manias, E.; Giannelis, E. P. *J. Chem. Phys.* **1998**, *108*, 7410.
(3) Okada, A.; Kawasumi, M.; Kojima, Y.; Kuraichi, T.; Kamigaito, O. *Mater. Res. Soc. Symp. Proc.* **1990**, *171*, 45.
(4) Yano, K.; Uzuki, A.; Okada, A.; Kuraichi, T.; Kamigaito, O. *J. Polym. Sci., Part A: Polym. Chem.* **1993**, *31*, 2493.
(5) Kojima, Y.; Uzuki, A.; Kawasumi, M.; Okada, A.; Kuraichi, T.; Kamigaito, O. *J. Polym. Sci., Part A: Polym. Chem.* **1993**, *31*, 983.

(6) Uzuki, A.; Kawasumi, M.; Kojima, Y.; Okada, A.; Kuraichi, T.; Kamigaito, O. *J. Mater. Res.* **1993**, *8*, 1174.
(7) Vaia, R. A.; Jandt, K. D.; Kramer, E. J.; Giannelis, E. P. *Macromolecules* **1995**, *28*, 8080.
(8) Lan, T.; Kaviratna, P. D.; Pinnavaia, T. J. *Chem. Mater.* **1995**, *7*, 2144.
(9) Vaia, R. A.; Sauer, B. B.; Tse, O. K.; Giannelis, E. P. *J. Polym. Sci., Part B: Polym. Phys.* **1997**, *35*, 59.
(10) Messersmith, P. B.; Stupp, S. I. *J. Mater. Res.* **1992**, *7*, 2599.
(11) Krishnamoorti, R.; Vaia, R. A.; Giannelis, E. P. *Chem. Mater.* **1996**, *8*, 1728.
(12) Vaia, R. A.; Giannelis, E. P. *Macromolecules* **1997**, *30*, 7990; **1997**, *30*, 8000.
(13) Asakura, S.; Oosawa, F. *J. Chem. Phys.* **1954**, *22*, 1255.
(14) Vrij, A. *Pure Appl. Chem.* **1976**, *48*, 471.
(15) Poon, W. C. K.; Selfe, J. S.; Robertson, M. B.; Illett, S. M.; Pirie, A. D.; Pusey, P. N. *J. Phys. II (Paris)* **1993**, *3*, 1075.
(16) Meijer, E. J.; Frenkel, D. *Phys. Rev. Lett.* **1991**, *67*, 1110.
(17) Lekkerkerker, H. N. W.; Poon, W. C. K.; Pusey, P. N.; Stroobants, A.; Warren, P. B. *Europhys. Lett.* **1992**, *20*, 559.
(18) Meijer, E. J.; Frenkel, D. *J. Chem. Phys.* **1994**, *100*, 6873.
(19) Gast, A. P.; Russel, W. B. *Phys. Today* **1998**, *12*, 24 and references therein.
(20) Illett, S. M.; Orrock, A.; Poon, W. C. K.; Pusey, P. N. *Phys. Rev. E* **1995**, *51*, 1344.
(21) Bolhuis, P. G.; Stroobants, A.; Frenkel, D.; Lekkerkerker, H. N. W. *J. Chem. Phys.* **1997**, *107*, 1551.
(22) Adams, M.; Dogic, Z.; Keller, S. L.; Fraden, S. *Nature* **1998**, *393*, 349 and references therein.
(23) Dijkstra, M.; van Roij, R. *Phys. Rev. E* **1997**, *56*, 5594.
(24) Dijkstra, M.; Hansen, J. P.; Madden, P. A. *Phys. Rev. E* **1997**, *55*, 3044.
(25) Lyatskaya, Y.; Balazs, A. C. *Macromolecules* **1998**, *31*, 6676.
(26) Onsager, L. *Ann. N. Y. Acad. Sci.* **1949**, *51*, 627.
(27) Brochard, F.; Jouffroy, J.; Levinson, P. *J. Phys. (Paris)* **1984**, *45*, 1125.
(28) Liu, A. J.; Fredrickson, G. *Macromolecules* **1993**, *26*, 2817.
(29) Chiu, H.-W.; Kyu, T. *J. Chem. Phys.* **1995**, *103*, 7471; *Phys. Rev. E* **1996**, *53*, 3618; *J. Chem. Phys.* **1997**, *107*, 6859.
(30) Somoza, A. M.; Tarazona, P. *J. Chem. Phys.* **1989**, *91*, 517.
(31) Tarazona, P. *Phys. Rev. A* **1985**, *31*, 2673.
(32) Ramakrishnan, T. V.; Yussouf, M. *Phys. Rev. B* **1979**, *19*, 2775.
(33) Kventsel, G. F.; Luckhurst, G. R.; Zewdie, H. B. *Mol. Phys.* **1985**, *56*, 589.
(34) Fleer, G.; Cohen-Stuart, M. A.; Scheutjens, J. M. H. M.; Cosgrove, T.; Vincent, B. *Polymers at Interfaces*; Chapman and Hall: London, 1993; Chapter 5.
(35) Singh, C.; Pickett, G. T.; Zhulina, E.; Balazs, A. C. *J. Phys. Chem. B* **1997**, *101*, 10614.
(36) Balazs, A. C.; Singh, C.; Zhulina, E. *Macromolecules* **1998**, *31*, 8370 and references therein.
(37) Ginzburg, V. V.; Singh, C.; Balazs, A. C., manuscript in preparation.
(38) Velasco, E.; Somoza, A. M.; Mederos, L. *J. Chem. Phys.* **1995**, *102*, 8107.
(39) Ginzburg, V. V.; Glaser, M. A.; Clark, N. A. *Liq. Cryst.* **1997**, *23*, 227.
(40) Carnahan, N. F.; Starling, K. E. *J. Chem. Phys.* **1969**, *51*, 635.
(41) Luckhurst, G. R.; Simmonds, P. S. J. *Mol. Phys.* **1993**, *80*, 233.
(42) Vroege, G. J.; Lekkerkerker, H. N. W. *Rep. Prog. Phys.* **1992**, *55*, 1241.
(43) The free energy βF_{int} includes both entropic and enthalpic contributions to the free energy of polymers in the "gallery" between the two sheets. Thus, the requirement that βF_{int} is small can be satisfied if there is an effective adsorption of chains on the clay surface. Here, the losses in the conformational entropy are balanced by the gains in enthalpy. For more details on the calculation of the free energy of adsorbing chains between the two surfaces, see refs 35 and 36.
(44) Frenkel, D. *Mol. Phys.* **1987**, *60*, 1.
(45) de Gennes, P. G.; Prost, J. *Physics of Liquid Crystals*; Oxford Science Publications: Oxford, 1993; Chapter 2.
(46) Calculations are performed on a Silicon Graphics workstation Indy R6000; one run takes approximately 1 h of CPU time.
(47) Sokolova, E. P.; Vlasov, A. Yu. *Liq. Cryst.* **1990**, *8*, 47.
(48) Clark, N. A.; Hurd, A. J.; Ackerson, B. J. *Nature* **1979**, *281*, 57.
(49) de Miguel, E.; Rull, L. F.; Chalam, M. K.; Gubbins, K. E.; van Swol, F. *Mol. Phys.* **1991**, *72*, 593; **1991**, *74*, 405.
(50) de Miguel, E.; del Rio, E. M.; Brown, J. T.; Allen, M. P. *J. Chem. Phys.* **1996**, *105*, 4234.
(51) Gay, J. G.; Berne, B. J. *J. Chem. Phys.* **1981**, *74*, 3316.
(52) Bates, M.; Luckhurst, G. R. *J. Chem. Phys.* **1996**, *104*, 6696.

MA990135T